Enhanced photocatalytic performance of V_2O_5 NRs/RGO nanocomposites for Rhodamine-B decolorization under solar irradiation

Experimental and theoretical study

Boukhoubza, Issam; Achehboune, Mohamed; El Khouja, Outman; Basyooni-M.Kabatas, Mohamed A.; Mindroc, Melania; Derkaoui, Issam; Enculescu, Monica; Matei, Elena

DOI
10.1016/j.jpcs.2025.112654

Publication date
2025

Document Version
Final published version

Published in
Journal of Physics and Chemistry of Solids

Journal of Physics and Chemistry of Solids 201 (2025) 112654

Contents lists available at ScienceDirect

Journal of Physics and Chemistry of Solids

journal homepage: www.elsevier.com/locate/jpcs

Enhanced photocatalytic performance of V_2O_5 NRs/RGO nanocomposites for Rhodamine-B decolorization under solar irradiation: Experimental and theoretical study

Issam Boukhoubza [a,b,*], Mohamed Achehboune [c,d], Outman El Khouja [a], Mohamed A. Basyooni-M. Kabatas [e,f], Melania Mindroc [a], Issam Derkaoui [b], Monica Enculescu [a], Elena Matei [a]

[a] National Institute of Materials Physics, Atomistilor 405A, Magurele, 077125, Romania
[b] Laboratory of Solid State Physics, Faculty of Sciences Dhar El Mahraz, University Sidi Mohammed Ben Abdellah, PO Box 1796, Atlas, Fez, 30 000, Morocco
[c] Laboratoire de Physique Du Solide, Namur Institute of Structured Matter, University of Namur, Rue de Bruxelles 61, 5000, Namur, Belgium
[d] School of Applied and Engineering Physics, University Mohammed VI Polytechnic, Ben Guerir, 43150, Morocco
[e] Department of Precision and Microsystems Engineering, Delft University of Technology, Mekelweg 2, 2628 CD, Delft, the Netherlands
[f] Department of Nanotechnology and Advanced Materials, Graduate School of Applied and Natural Science, Selçuk University, Konya, 42030, Turkey

ARTICLE INFO

Keywords:
V_2O_5/RGO nanocomposites
Hydrothermal method
Photocatalytic activity
DFT

ABSTRACT

In the present work, an essential advance in the preparation of novel nanocomposites based on functionalized V_2O_5 nanostructures with reduced graphene oxide by hydrothermal method, which has great potential for use in photocatalytic processes related to environmental remediation. XRD analysis confirmed V_2O_5 in an orthorhombic structure. SEM images showed transparent RGO layers well anchored onto the surface of the V_2O_5 with a homogeneous distribution. Raman spectroscopy further explained the hybridization and interaction between the components. The photocatalytic activity of Rhodamine-B in aqueous solutions has been studied upon irradiation with visible light. A high RhB degradation was obtained using the V_2O_5/RGO photocatalyst (82 %), compared to the degradation obtained with only V_2O_5 (60 %). First-principles Density Functional Theory (DFT) simulations reveal a strong interaction between V_2O_5 molecules and graphene surfaces, with an adsorption energy of −1.673 eV and a significant charge transfer of 0.367 e− to RGO. This interaction modifies the electronic structure, creating semi-metallic behavior near the Fermi level and enhancing catalytic activity through improved charge carrier dynamics and active sites for photocatalytic applications.

1. Introduction

The industrial sector has become an essential engine for economic development. However, this improvement is accompanied by the negative consequence of manufacturing many types of waste that significantly influence the environment, particularly the discharge of organic pollutants [1–3]. In this context, dyes such as methylene blue, Rhodamine B (RhB), and crystal violet, as well as organic pollutants including salicylic acid, phthalic acid, and Eriochrome Black-T, have received enormous attention owing to their extensive usage and the challenges associated with their degradation [4–10]. These compounds have a wide range of applications in various industries, including food, cosmetics, pharmaceuticals, and textiles. By their molecular structure, these dyes are resistant toward biodegradation and other forms of degradation. Rhodamine B was selected for research since it presents fluorescent properties and allows for easy and accurate degradation rate measurements [11]. This dye has a high solubility in water and is commonly used in textile, cosmetic, and food industries [12,13]. Due to the RhB dye's toxic characteristics [14,15], further attempts should be made to find effective methods for removing RhB dye from wastewater and treating industrial waste.

Various physical and chemical methods have been applied to remove dyes from wastewater, including adsorption, filtration, and degradation. Among these, photocatalytic degradation of dyes has exhibited the highest efficiency due to its low energy consumption, cost-effectiveness, and ability to handle large volumes of wastewater [16]. In

* Corresponding author. National Institute of Materials Physics, Atomistilor 405A, Magurele, 077125, Romania.
E-mail address: boukhoubza.issam00@gmail.com (I. Boukhoubza).

https://doi.org/10.1016/j.jpcs.2025.112654
Received 16 December 2024; Received in revised form 22 February 2025; Accepted 25 February 2025
Available online 28 February 2025

photocatalytic degradation, a light source and semiconductor materials work together to generate hydroxyl radicals, which then decompose organic molecules [17]. Currently, different types of metal oxide nanostructures and their nanocomposite-based graphene derivatives have been employed in efforts toward the advancement of sustainable photocatalytic technologies. Among these semiconductor catalysts, Vanadium pentoxide (V_2O_5) has attracted increasing interest owing to its advantageous properties, such as a visible band gap energy of around 2.3–2.9 eV, high exciton energy (519 meV), an extensive surface area with a straightforward synthesis of different related nanostructures [5,18]. While V_2O_5 acts as a very active photocatalyst, its action is often hindered by one or more of the following factors: a high rate of charge carrier recombination, a low capacity for adsorption of hydrophobic pollutants, a tendency to aggregate, and a transformation of absorbed energy into heat reduce photocatalytic efficiency [19–21].

The combination of V_2O_5 with graphene derivatives has recently received much attention in the scientific community to achieve higher activity. Reduced graphene oxide-based photocatalyst nanocomposites enabled the availability of high surface area, abundant functional surface groups, superior electrical conductivity, strong thermal stability, enhanced charge transfer efficiency, and improved photogenerated charge carrier mobility in the photocatalytic approach with variable bandgap [22,23].

Various methods have been employed to synthesize V_2O_5/RGO nanocomposites in order to enhance their photocatalytic performance. For example, Yadav et al. [4] utilized a hydrothermal process to prepare V_2O_5/RGO composites for the photocatalytic degradation of methylene blue (MB) dye. Top et al. [24] explored the relationship between electron-hole pair separation, diffusion, recombination, and degradation in V_2O_5 nanospheres and nanohollows/RGO composites, which were fabricated using wet chemical and hydrothermal methods. Deepanshu et al. [25] demonstrated the synthesis of reduced graphene oxide coupled with vanadium pentoxide nanocomposites via a simple hydrothermal route, validating their potential for MB dye photodegradation and photoelectrochemical (PEC) water-splitting applications. Furthermore, Pankaj et al. [5] reported the effective degradation of Rhodamine B (RhB) dye using V_2O_5/RGO nanocomposites through the Advanced Oxidation Process (AOP). Additionally, Denh et al. [26] developed a CeO_2–V_2O_5/RGO photocatalytic system for the photodegradation of cefotaxime in aqueous solutions.

This work produced, V_2O_5 nanorods (NRs) and V_2O_5/RGO nanocomposites using hydrothermal process. All the characterizations have been performed using several techniques such as X-ray diffraction, scanning electron microscopy, Raman spectroscopy as well as UV–visible spectroscopy, to study the influence of RGO on the structural, morphological, vibrational, and optical characteristics of V_2O_5 nanorods within the nanocomposites. Further, the photocatalytic activity of V_2O_5/RGO nanocomposites was also investigated, as well as the degradation of Rhodamine B dye under sunlight irradiation. Furthermore, density functional theory has been employed to theoretically examine the interaction and comprehend the complex relationship between these nanocomposites' interface structure and electronic properties. This research advances our understanding of the photocatalytic applications and fundamental features of V_2O_5/RGO nanocomposites, addressing the need for both theoretical modeling and experimental validation in this intriguing field.

2. Synthesis method

2.1. Synthesis of V_2O_5 NRs, RGO and V_2O_5 NRs/RGO nanocomposites

Vanadium pentoxide (V_2O_5) nanorods were produced using a hydrothermal approach. In the first step, Ammonium metavanadate (NH_4VO_3) was calcined at 500 °C for 2 h to synthesize bulk V_2O_5. After that, a yellow slurry solution was formed by dissolving 750 mg of V_2O_5 obtained in 120 mL of deionized (DI) water. Next, an orange-red solution was achieved after stirring 10 mL of a dropwise added slurry solution containing 30 % hydrogen peroxide (H_2O_2) for 2 h. In the second step, the mixture was then put in a Teflon autoclave with a capacity of 200 mL and heated at 160 °C for 24 h at a heating rate of 10 °C/min using a controlled oven. After cooling down naturally from the autoclave to average room temperature, the resulting precipitate was filtrated from the solution, cleaned with ethanol and DI water to purify it, and then allowed to air at 90 °C for 6 h.

To produce GO, pure graphite was first treated with a modified Hummers' process [27], which required treatment with sulfuric acid (H_2SO_4) and potassium permanganate ($KMnO_4$). The resulting GO served as the precursor for synthesizing reduced graphene oxide (RGO). This reduction was attained by chemically treating the GO with 60 μL of hydrazine hydrate at 50 °C while stirring the mixture continuously for 24 h.

The V_2O_5 nanorods/RGO nanocomposites were prepared using the same procedure as pure V_2O_5. First, 10 mg of as-synthesized V_2O_5 nanorods were mixed in 10 mL of DI water, and then the RGO with different concentrations (4 %, 6 %, and 8 %) was dissolved in 10 mL of DI water and sonicated for 1 h. The two solutions were combined and transferred to the 50 mL hydrothermal autoclave, treated at 120 °C for 12 h. Finally, the as-obtained V_2O_5 NRs/RGO nanocomposites were filtered and washed several times using DI water. Fig. 1 illustrates the different steps in synthesizing V_2O_5 NRs/RGO nanocomposites.

2.2. Characterization

The crystalline characteristics of the synthesized nanocomposites were determined by XRD analysis. The Measurements were conducted on an X-ray diffractometer (D8 Bruker AXS, Karlsruhe, Germany) with CuKα radiation (λ = 1.54178 Å) in the 2θ range from 20° to 70°.

Morphological investigation was performed using a Zeiss Gemini 500 field emission scanning electron microscope (Oberkochen, Germany) equipped with a Bruker energy dispersive X-ray detector (EDX) (Karlsruhe, Germany). The vibrational modes of the synthesized samples were obtained using a Raman spectrometer (Horiba Jobin-Yvon: Edison, USA) and further analyzed using a He–Ne laser emitting at the $\lambda_{Exc} = 633$ nm. The laser beam was focused on the sample surface through an Olympus 100 × objective lens. Surface analyses were performed using X-ray photoelectron spectroscopy (XPS). The measurements were conducted with a Thermo VG system (UK), utilizing a monochromatic Al Kα source emitting at 1486.6 eV to provide detailed insights into bonding characteristics and impurities. The optical properties of the prepared nanocomposites were performed using a UV–Vis spectrophotometer, PerkinElmer Lambda 45 (Waltham, MA, USA).

The degradation of Rhodamine B in an aqueous solution exposed to visible light irradiation at room temperature was monitored to evaluate the photocatalytic activity of V_2O_5 nanorods and its nanocomposite. For each experiment, 5 mg of catalyst (V_2O_5 or V_2O_5/6%RGO) was added to a beaker containing 10 mL of 10^{-5} M RhB solution. The reaction mixtures were positioned 10 cm from the light source, an SF300-A Small Collimated Beam Solar Simulator with a 300 W Xe lamp (Sciencetech, London, Canada), during the optical measurements. At various time intervals during irradiation, the optical absorbance spectra of the samples at wavelengths between 400 and 700 nm were measured using a UV–Vis spectrophotometer (Varian, GmbH, Waldbronn, Germany) equipped with a quartz cell with a 10 mm light path.

The degradation efficiency of RhB was evaluated by taking samples after a specific interval of irradiation times. The following formula determined the performance of the samples for pollutant degradation:

$$D\% = \left(\frac{C_0 - C}{C_0}\right) \times 100, \quad (1)$$

where C_0 is the dye's initial absorbance at $\lambda_{max,}$ and C is the absorbance of the dye a particular duration of time. The results revealed the

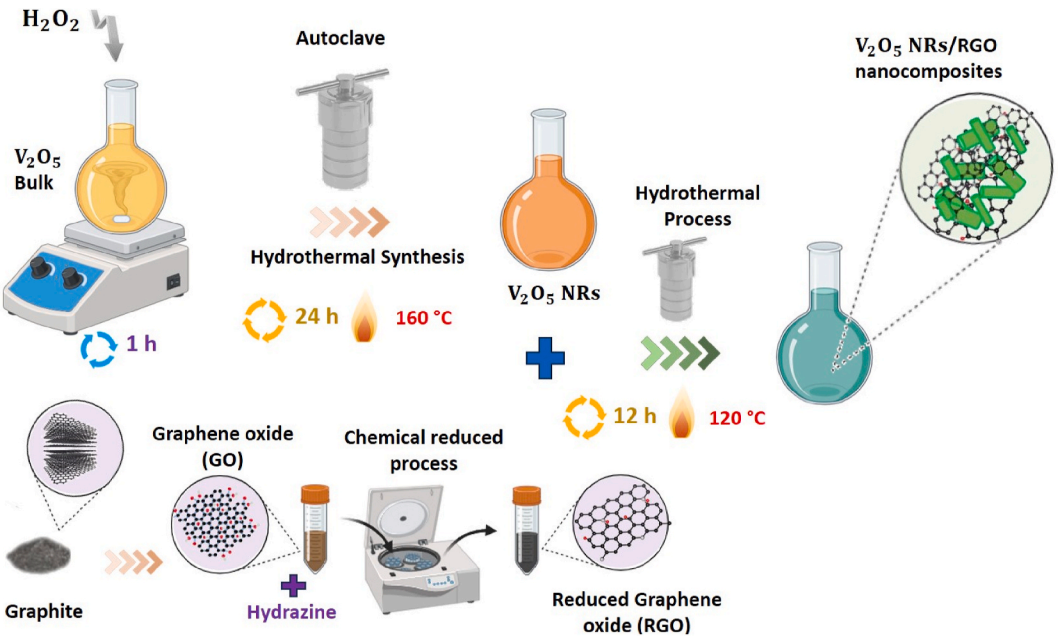

Fig. 1. Representation of V_2O_5 NRs, RGO, and V_2O_5 NRs/RGO nanocomposites growth by hydrothermal process.

reduction of RhB concentration during the photoreduction process.

2.3. Computational method

In this investigation, structural simulations and property evaluations were carried out using spin-polarized Density Functional Theory (DFT) as integrated in the Vienna Ab Initio Simulation Package (VASP) [28,29]. The projector-augmented wave (PAW) method was applied to model ion-electron interactions [30], and the exchange-correlation energy of interacting electrons was represented using the Perdew–Burke–Ernzerhof (PBE) functionals under the generalized gradient approximation (GGA) [31]. To consider van der Waals interactions between the V_2O_5 molecule and the graphene surface, the D3 semi-empirical correction by Grimme [32] was employed. The plane-wave cut-off energy and k-point mesh were optimized to achieve total energy convergence to 10^{-3}eV per atom. A kinetic energy cut-off of 500 eV was used for all computations involving 4 × 4 supercell structures, along with a 6 × 6 × 1 Γ Monkhorst–Pack grid for Brillouin zone sampling. To eliminate interactions between periodic images in the z-direction, a vacuum layer of 15 Å was included. The standards for electronic and ionic convergence were established at 10^{-5}eV and 10^{-3} eV, respectively.

The adsorption energy (E_{ads}) of V_2O_5 on the reduced graphene oxide surface was calculated as:

$$E_{ads} = E_{V_2O_5+RGO} - (E_{RGO} + E_{V_2O_5}), \quad (2)$$

where $E_{V_2O_5+RGO}$ is the total energy of the V_2O_5/RGO system, E_{RGO} is the energy of the isolated reduced graphene oxide layer, and $E_{V_2O_5}$ is the energy of the isolated V_2O_5 molecule.

Charge density differences ($\Delta\rho$) were calculated using:

$$\Delta\rho = \rho(V_2O_5 + RGO) - (\rho(RGO) + \rho(V_2O_5)) \quad (3)$$

where $\rho(V_2O_5 + RGO)$, and $\rho(RGO)$ and $\rho(V_2O_5)$ the charge densities of the combined system are bare, reduced graphene oxide, and isolated V_2O_5, respectively. Finally, Bader charge analysis was conducted using the Henkelman algorithm [33] to quantify charge transfer at the interface.

3. Results and discussion

3.1. Structural properties

The structural characteristics of V_2O_5 bulk, V_2O_5 NRs and V_2O_5 NRs/RGO nanocomposites with varying RGO concentrations (4 %, 6 %, and 8 %) are examined using X-ray diffraction plots illustrated in Fig. 2. All the samples show diffraction peaks at about 2θ = 15.3°, 20.7°, 21.6°, 26.0°, 30.9°, 32.3° and 41.1°. These peaks correspond to the orthorhombic structure of the V_2O_5 phase in the (200), (001), (101), (110), (301), (011), and (002) planes [34,35] according to ICDD PDF card no. 00-041-1426 [36], with space group 59: Pmmn, and the determined lattice parameters were a = 11.543 Å, b = 4.382 Å and c = 3.570 Å. The intensity of the (001) diffraction peak increases significantly in the case of nanocomposites, suggesting an enhanced crystalline nature of the V_2O_5 NRs.

It can also be observed that the characteristic peaks intensity of nanocomposites decreases in comparison with V_2O_5 NRs, and the distinct peak of RGO which is typically situated at 2θ = 23°, could not be noticed in nanocomposites. The reduced intensity may be attributed to the dispersion of RGO over V_2O_5, resulting in only the visibility of V_2O_5 peaks in the nanocomposite due to the small quantity of RGO within the sample, respectively.

Based on the full-width-at-half-maximum (FWHM) of the diffraction peak positions, the average crystallite size and micro-strain (ε) of the V_2O_5 nanorods and V_2O_5 NRs/RGO nanocomposites were calculated using the Debye–Scherrer and Williamson–Hall (W–H) formulas, as given in Equations (4) and (5), respectively [37,38].

$$D = \frac{k\lambda}{\beta \cos\theta} \quad (4)$$

$$\beta \cos\theta = \frac{K\lambda}{D} + 4\varepsilon \sin\theta \quad (5)$$

Where β is the full width at half maximum (FWHM) of the X-ray peak, θ is the Bragg angle, λ is the X-ray wavelength (λ = 1.54178 Å, CuKα radiation), and K = 0.9 is Scherer's factor. In addition, ε is microstrain and D is the crystallite size. The average crystallite size decreased from 82 to 64 nm with increasing RGO content, while the microstrain varied with crystallite size. The values from the Williamson-Hall method were

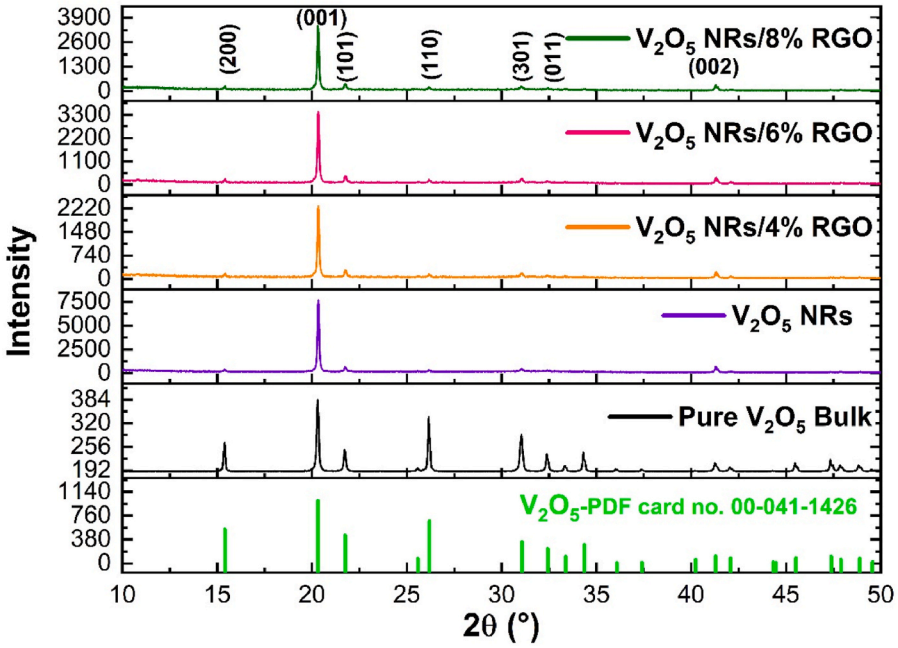

Fig. 2. XRD spectra of V_2O_5 bulk, V_2O_5 nanorods and V_2O_5 NRs/RGO nanocomposites at different concentrations of RGO (4 %, 6 % and 8 %).

consistently larger than those from the Scherrer (Table 1).

3.2. SEM and EDX

The morphology of the V_2O_5 bulk powder, V_2O_5 NRs and V_2O_5 NRs/RGO nanocomposites was analyzed using SEM images. Fig. 3a shows that the V_2O_5 bulk powder has an average particle size of 200 nm, with its shape and size influenced by the reaction temperature and time during synthesis process. The SEM images depict V_2O_5 NRs, both in their pure form and within nanocomposites. They display a high-density growth with an average length of approximately 60–100 nm and a diameter of about 15 nm (Fig. 3b). In the case of low concentration (Fig. 3c), a few transparent layers of RGO were anchored and evenly distributed on the V_2O_5 nanorods' surface. Conversely, SEM images with higher RGO concentration (Fig. 3d–e) illustrate that RGO layers covered the surfaces of V_2O_5 nanorods. Some of these V_2O_5 nanostructures are anchored on RGO (Fig. 3e), indicating a strong interaction between V_2O_5 nanorods and RGO layers. The findings show that V_2O_5 NRs/RGO nanocomposites were successfully formed.

The uniformity in composition of both vanadium pentoxide nanorods and V_2O_5 NRs/RGO nanocomposites on ITO substrates was investigated using EDX mapping (Fig. 4). The first row of SEM fields displays the areas where element mapping for carbon, oxygen, vanadium, silicon, indium, and tin was conducted. In the case of V_2O_5 NRs/RGO nanocomposites, the presence of vanadium, oxygen, carbon and other elements belonging to the substrate was observed, with no detection of other elements in the nanocomposites. Additionally, EDX mapping analyses revealed an increase in carbon intensity in certain areas in the case of samples in which RGO was present. These results align well with the expected chemical composition, confirming the successful synthesis of V_2O_5 NRs/RGO nanocomposites.

Table 1
Average crystallite size of V_2O_5 NRs, and V_2O_5 NRs/RGO nanocomposites.

Samples	Scherrer method		Williamson-Hall method	
	Average Crystallite Size (nm)	Dislocation density (δ) (10^{-4})	Crystallite Size (nm)	Microstrain (10^{-3})
V_2O_5 NRs	74.06	1.826	82.57	4.32
V_2O_5 NRs/ 4%RGO	67.32	2.220	72.52	4.30
V_2O_5 NRs/ 6%RGO	66.83	2.234	65.82	4.28
V_2O_5 NRs/ 8%RGO	63.95	2.449	64.35	4.29

3.3. Raman and XPS analysis

Raman measurements (Fig. 5) provided vibrational information for V_2O_5 NRs and V_2O_5 NRs/RGO. The Raman spectrum analysis of V_2O_5 (Fig. 5a) exhibited characteristic bands at 144, 194, 282, 405, 481, 526, 692, and 996 cm^{-1}. Specifically, the bands at 144 cm^{-1} and 194 cm^{-1} were assigned to the layered structure of orthorhombic V_2O_5 (B_{3g} mode)) and the V–O stretching mode (B_{1g} symmetry), respectively. The bands at 282 and 405 cm^{-1} were linked to the bending vibration of the V═O bonds (B_{2g} and A_g symmetry modes) [39,40]. The band at 526 cm^{-1} corresponded to the V_3–O stretching mode (Ag symmetry) [39, 40]. The band observed at 692 $cm^{-1}$was attributed to the V_2–O bond bending vibration (B_{2g} symmetry mode), while the band at 996 cm^{-1} coincided with the terminal oxygen (V═O) stretching vibration in the A_{1g} and B_{2g} symmetry modes [36,41]. The band at 1046 cm^{-1} is also associated with vanadyl oxygen (V^{5+}═O), stretching mode [42].

In Fig. 5b, the Raman spectra of the V_2O_5 NRs/RGO nanocomposite, at different concentrations of RGO, exhibit multiple vibration bands characteristic of the V_2O_5 phase, and two distinct bands appeared around 1365 and 1598 cm^{-1}, identified as D and G bands, respectively. These bands confirm the existence of reduced graphene oxide, a feature strongly linked to carbon materials. The D band (1365 cm^{-1}) corresponds to sp^2 hybridized carbon atoms, while the G band (1598 cm^{-1}) is associated with vibrations of sp^3 carbon atoms, defects, and disorders in graphitic materials [43]. The presence of these two bands provides additional evidence for the integration of reduced graphene oxide in the V_2O_5 nanocomposite. The I_D/I_G intensity ratio is a crucial parameter for evaluating the defects and the average size of sp^2 domains in carbon materials. It performs a significant role in assessing the level of graphitization [44]. The calculated I_D/I_G ranged from 0.89 to 0.99 as the nanocomposite's RGO content increased from 4 to 8 %. This result suggests that introducing RGO into the V_2O_5 network does not induce substantial defects in the nanocomposite. Additionally, it indicates an

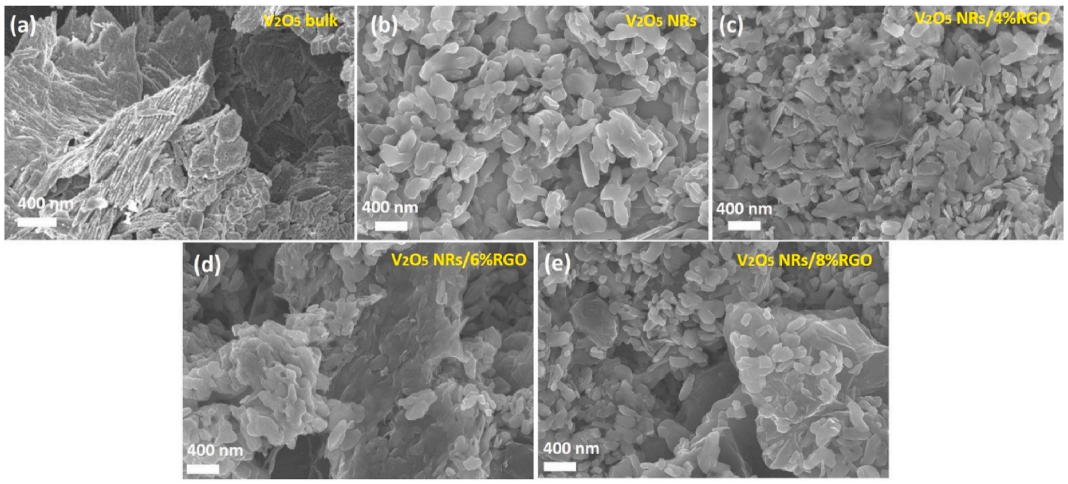

Fig. 3. SEM images of (a) V_2O_5 bulk, (b) V_2O_5 NRs and (c–e) V_2O_5 NRs/RGO nanocomposites at different concentrations of RGO (4 %, 6 %, and 8 %).

enlargement in the size of sp^2 domains and the restoration of a carbon structure during the hydrothermal process.

Furthermore, the average crystallite size (La) was determined using the I_D/I_G ratio determined from the Raman spectra, following the equation described in reference [45]:

$$L\,a\ \ (nm) = \left(2.4 \times 10^{-10}\right)\lambda^4 \left(\frac{I_D}{I_G}\right)^{-1}, \tag{6}$$

where $\lambda = 633$ nm and represents the wavelength of the laser excitation. The calculated values for the V_2O_5 NRs/4 % RGO, V_2O_5 NRs/6 % RGO, and V_2O_5 NRs/8 % RGO nanocomposites were 43.29 nm, 39.72 nm, and 38.92 nm, respectively.

Fig. 5c-e XPS analysis of the V_2O_5/RGO nanocomposite shows the presence of V 2p, O 1s, and C 1s elements. The high-resolution V $2p_3/_2$ and V $2p_1/_2$ peaks attributed to V^{5+} appear at 517.15 and 525.12 eV, respectively. Those corresponding to V^{4+} are located at 516.11 and 523.83 eV [46] (Fig. 5c). Additionally, the O 1s spectrum is deconvoluted into two peaks at 530.6 and 531.4 eV that can be assigned to V–O and V–OH bonds, respectively (Fig. 5d) [47]. Moreover, the C 1s spectrum shown in Fig. 5e is deconvoluted into two peaks located at 284.5 and 285.9 eV, which are assigned to C–C and C–O bonds of reduced graphene oxide and its functional groups [48].

3.4. Density functional theory simulation

In this simulation part, we used the first principal calculations based on Density Functional Theory (DFT) to study at atomic scale the interaction between reduced graphene oxide surface and V_2O_5 molecule interfaces in terms of lattice stability, electron Density of States (DOS) and interfacial/surface charge transfer. Schematic illustrations for the clean RGO support, a molecule of V_2O_5 on the RGO layer (top view) alongside with charge plane-averaged charge density difference are shown in Fig. 6a. Table 2 illustrates the summary of the adsorbed energy and overall charge transfer among the adsorbed V_2O_5 molecule and RGO surface. The adsorption energy of V_2O_5 on graphene RGO is calculated to be −1.673 eV, showing a strong interaction between the molecule and the surface. This interaction results in a significant charge transfer of 0.367 e^- from the V_2O_5 molecule (adsorbate) to the RGO surface, as evidenced by the charge density difference analysis. This charge transfer modifies the electronic properties of the RGO surface, potentially enhancing its catalytic or sensing performance.

The electronic Density of States (DOS) analysis (Fig. 7a-c) reveals that the V_2O_5/RGO hybrid exhibits semi-metallic behavior, characterized by finite DOS at energy levels near the Fermi level (E_F). This finite DOS at E_F significantly contributes to the total DOS and indicates enhanced electronic activity. Interestingly, this behavior changes slightly, suggesting robust electroactive properties and improved active sites for catalytic or electronic applications. Furthermore, the Partial Density of States (PDOS) calculations indicate that the conduction band minimum is predominantly governed by contributions from vanadium (V) d-orbitals, with additional contributions from oxygen (O) 2p-orbitals, highlighting the synergistic interaction between vanadium and oxygen states in the hybrid structure. Fig. 6b, which illustrates the charge density difference, shows electrons accumulate on the RGO layer while V_2O_5 exhibits electron depletion, which may significantly enhance the photocatalytic efficiency.

Excited electrons in the conduction band react with oxygen molecules (O_2) to produce superoxide radical anions ($O_2^{-\bullet}$) through:

$$O_2 + e^- \rightarrow O_2^{-\bullet} \tag{7}$$

These radicals can further interact with protons (H^+) to produce hydroperoxy radicals ($HO_2^{\bullet}$), which combine with O_2 to generate hydrogen peroxide (H_2O_2) as:

$$O_2^{-\bullet} + H^+ \rightarrow HO_2^{\bullet} \tag{8}$$

$$2HO_2^{\bullet} \rightarrow H_2O_2 + O_2 \tag{9}$$

Simultaneously, valence band holes react with water (H_2O) to produce hydroxyl radicals ($OH^{\bullet}$) as:

$$H_2O + h^+ \rightarrow OH^{\bullet} + H^+ \tag{10}$$

These highly reactive radicals attack Rhodamine-B (RhB) molecules, breaking them into non-toxic byproducts like carbon dioxide (CO_2) and water (H_2O). The graphene's high conductivity enhances electron mobility, thus stabilizing reactive oxygen species (ROS) and improving catalytic activity. Furthermore, reduced graphene oxide (RGO) layers suppress charge recombination and enhance dye adsorption due to their high surface area, enabling efficient ROS-mediated degradation of RhB into environmentally benign products.

3.5. Optical properties

Fig. 8 illustrates a Tauc plot of V_2O_5 and V_2O_5 NRs/RGO nanocomposites to visualize the shift in bandgap energy. The band gaps were determined using the following equation [49]:

$$\alpha h\nu = \left(h\nu - E_g\right)^{1/2} \tag{11}$$

where E_g is the bandgap energy, $h\nu$ is the photon energy, and α is the absorption coefficient.

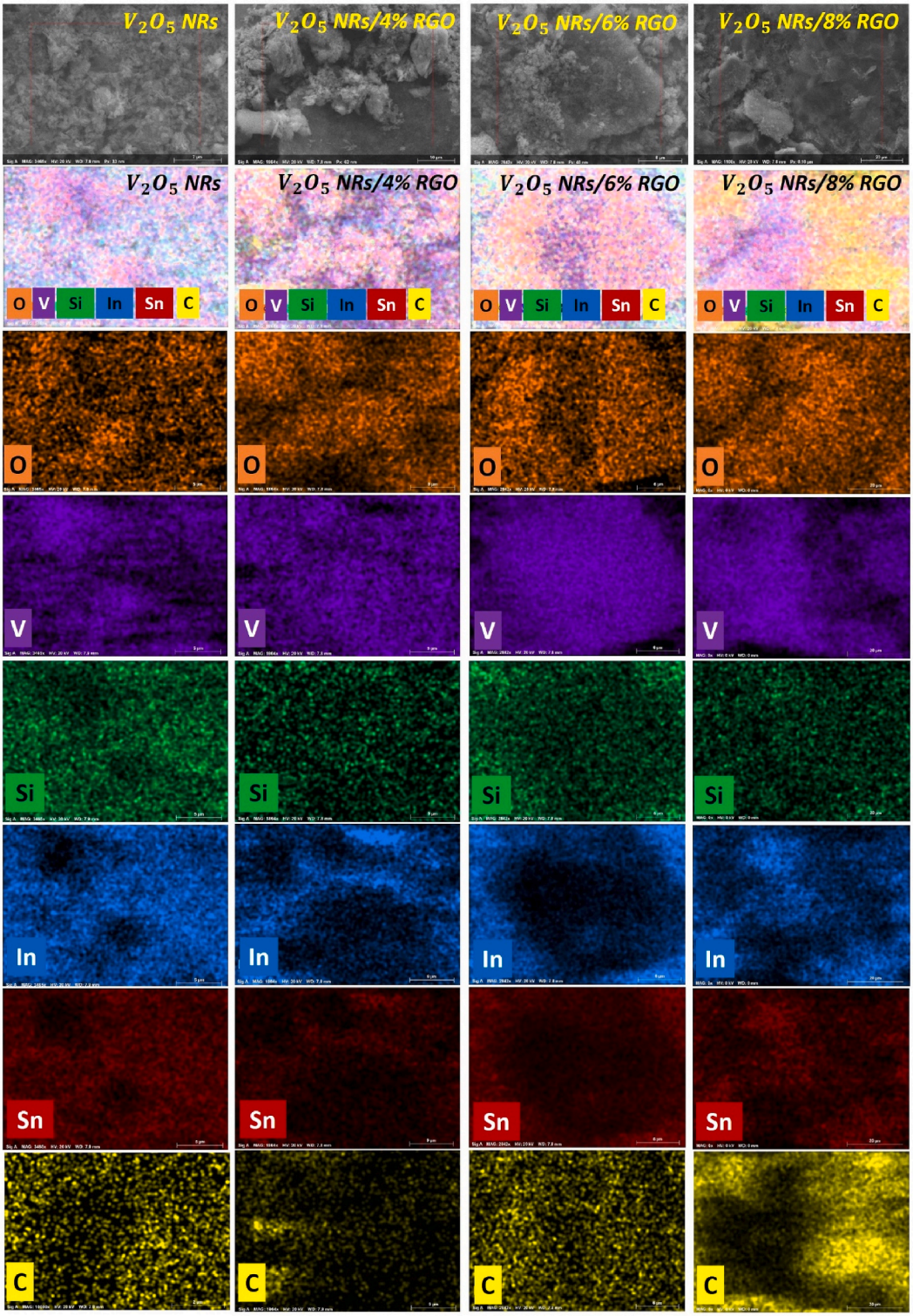

Fig. 4. EDX maps of V_2O_5 NRs and V_2O_5 NRs/RGO nanocomposites at different concentrations of RGO (4 %, 6 % and 8 %), on substrate of ITO.

As shown in Fig. 8, the band gap of V_2O_5 nanorods is 2.78 eV, while the V_2O_5 NRs/RGO nanocomposites have a band gap of 2.74, 2.45 and 2.30 eV for RGO concentrations of 4 %, 6 %, and 8 %, respectively. The reduction in the band gap with increased RGO concentration in the nanocomposites compared to V_2O_5 nanorods indicates higher optical absorption for V_2O_5 NRs/RGO. This implies that V_2O_5 NRs/RGO helps to improve the material's photocatalytic activity.

3.6. *Photocatalysis part*

The V_2O_5 NRs/6 % RGO nanocomposite was prepared and evaluated as a catalyst for the decolorization of RhB under solar white light radiation through photocatalytic activity measurement. The UV–visible absorbance spectra of a 10 mg/L RhB dye solution were analyzed over time during the photocatalytic reaction. Pure V_2O_5 NRs (5 mg) achieved approximately 60 % decolorization of a 10 mL RhB dye solution in 240

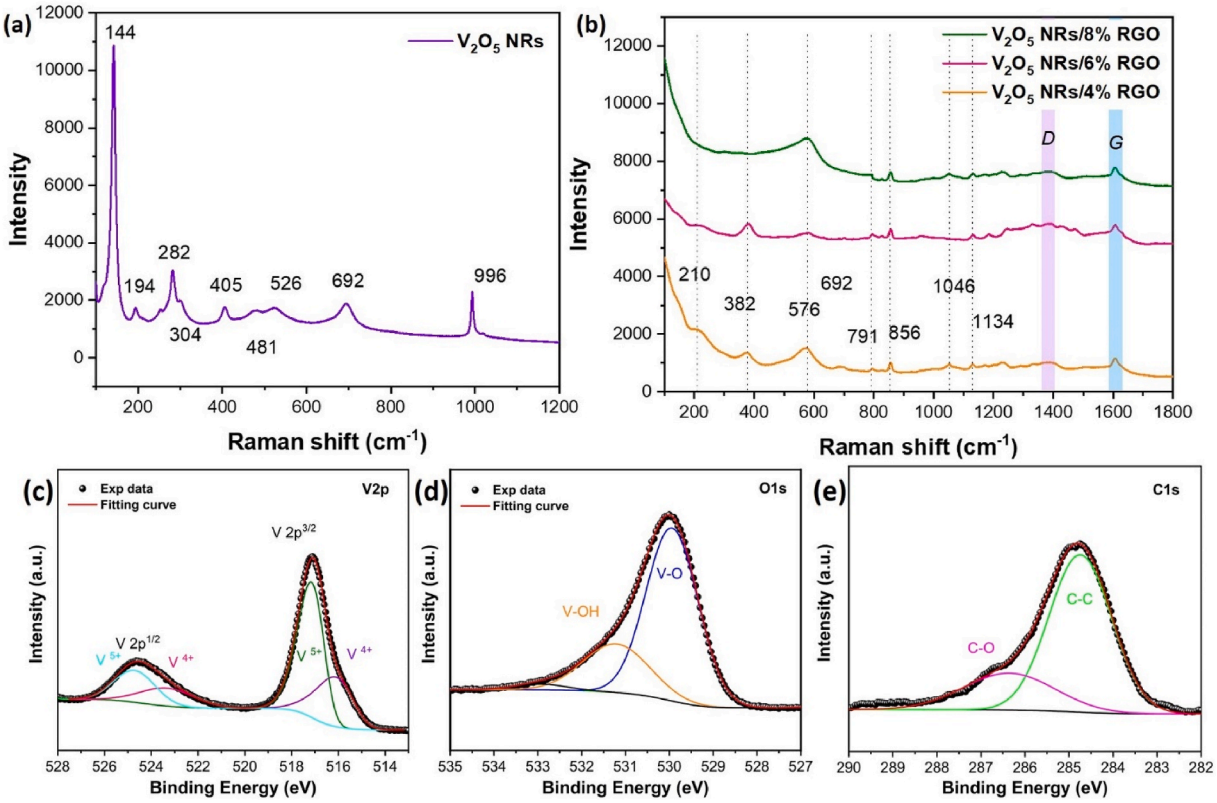

Fig. 5. Raman spectra of (a) V_2O_5 NRs and (b) V_2O_5 NRs/RGO nanocomposites at different concentrations of RGO (4 %, 6 %, and 8 %). XPS spectra of V_2O_5 NRs/RGO nanocomposites with high resolution XPS peaks for (c) V 2p, (d) O 1s, and (e) C 1s.

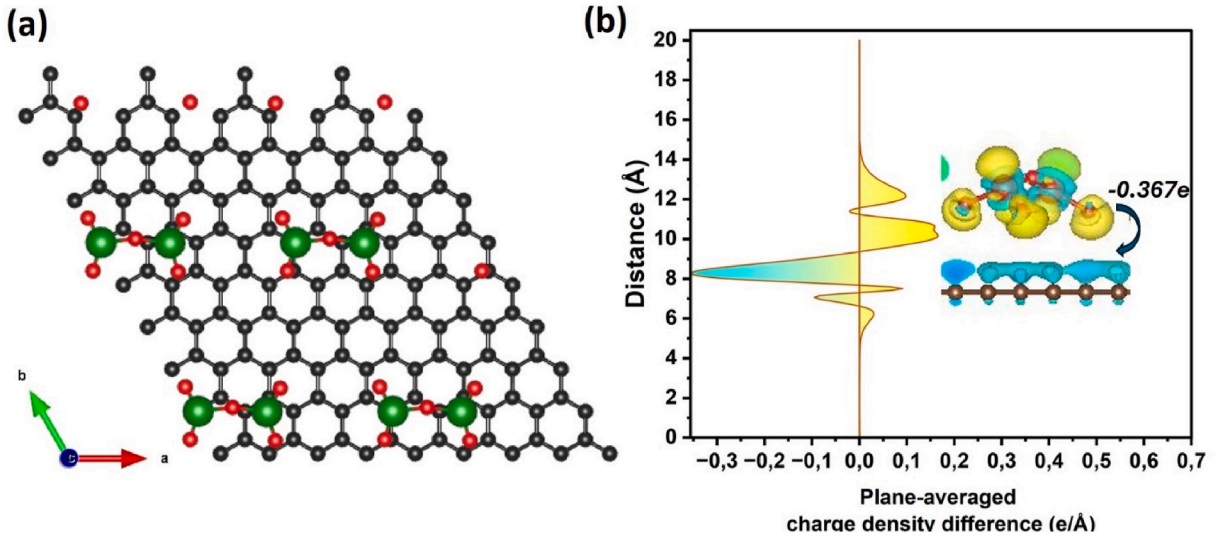

Fig. 6. (a) Schematic of V_2O_5 cluse adsorbed on reduced graphene oxide (top view) and (b) plane-averaged charge density difference.

min, respectively (Fig. 9a and c), while the V_2O_5 NRs/6 % RGO nanocomposite (10 mg) accomplished 82 % decolorization within the same time (Fig. 9b and c), this emphasizes the crucial role played by the RGO layer in nanocomposites. The presence of functional groups, such as carboxyl (-COOH) and hydroxyl (-OH), enhances the surface characteristics of RGO. Incorporating it into nanocomposites improves surface oxygen levels, reduces the bandgap, increases light absorption, and improves the electronic properties of V_2O_5 nanorods. Moreover, the combination of a large surface area and these functional groups' existence facilitates and promotes dye molecule adsorption. When comparing the photocatalytic performance of V_2O_5/RGO nanocomposites for the degradation of MB and RhB dyes in previous studies (Table 3), the performance of our nanocomposites in this work is commendable.

The mechanistic details of this photocatalytic degradation process are as follows (Fig. 9d). The dye molecules move to the catalyst surface and engage in redox reactions with other surface-bound species. When photon energy exceeds or equals the bandgap energy of 2.86 eV, the electrons in the VB band absorb enough energy. They become excited and transition to the CB, resulting in holes (h^+) in the valence band. The

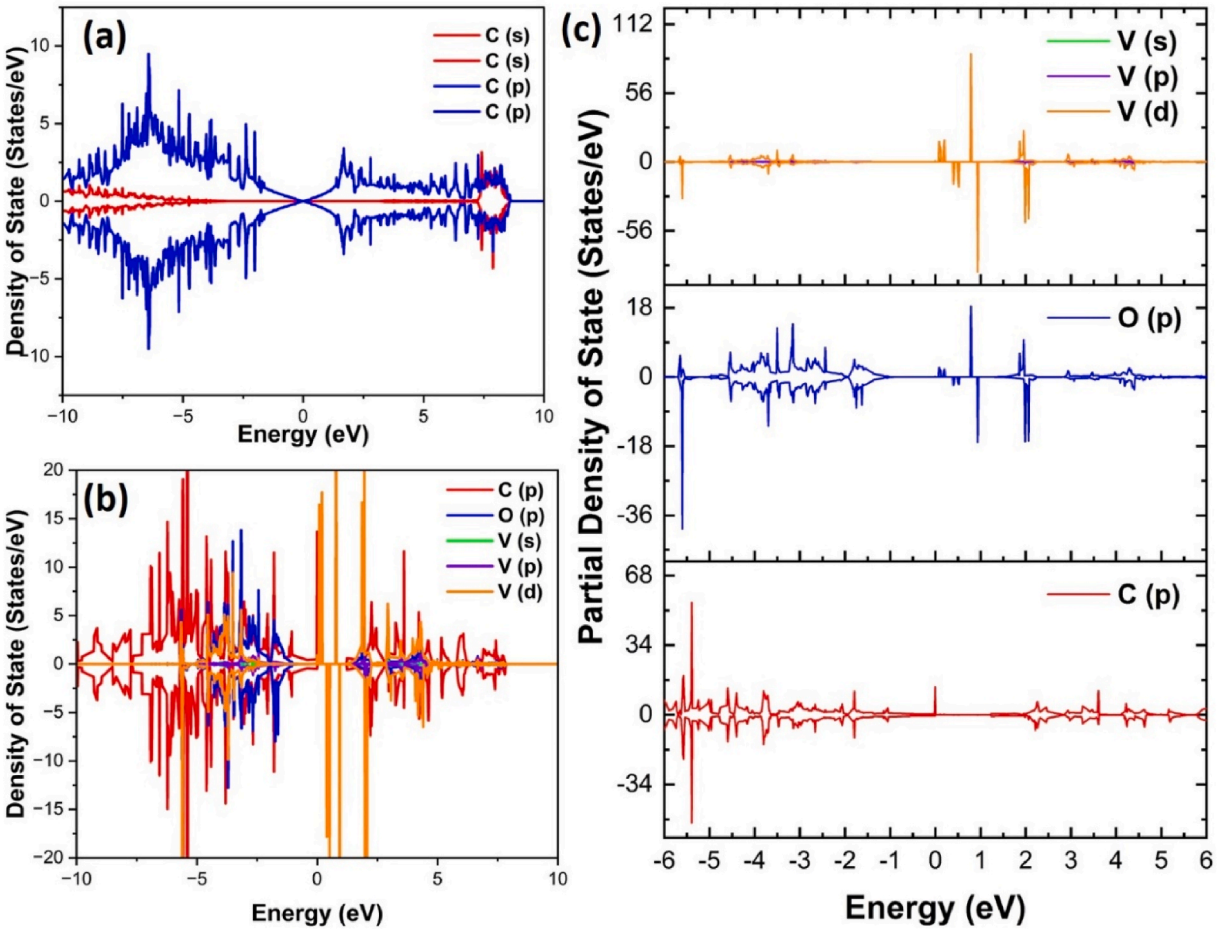

Fig. 7. Total and partial density of state spectra for (a) clean reduced graphene oxide surface, (b) and (c) V_2O_5 on RGO.

Table 2
Adsorption energy and charge Transfer of V_2O_5/RGO nanocomposite.

Structure	Adsorption Energy (eV)	Charge Transfer
V_2O_5/RGO	−1.673	−0.367e

excited CB electrons can react with oxygen (O_2) molecules to form superoxide radical anions (O_2^-*), which can further interact with H^+ ions to produce hydroperoxy (HO_2*) radicals. These radicals subsequently combine with oxygen to generate hydrogen peroxide (H_2O_2). In parallel, VB holes can react with water (H_2O) to form hydroxyl radicals (OH•). These reactive superoxide and hydroxyl radicals prevent electron-hole recombination and can break down dye molecules into non-toxic chemicals [18,53,54]. In this context, RGO layers reduce charge carrier recombination, improve charge transfer, and boost photocatalytic efficiency. As a result, hydroxyl radicals turn Rhodamine B molecules into carbon dioxide (CO_2), H_2O, and other low-concentration decomposition products. In addition, the nature of predominant reactive oxidizing species (ROS) for RhB degradation with metal oxide/graphene derivative will be different according to specific characteristics of the material. Chauhan et al. [5] demonstrated that in V_2O_5/rGO composites, hydroxyl radicals (•OH) dominate the degradation process due to the generation of hydroxyl free radicals through the reaction of OH^- ions with holes (h^+), facilitated by the high surface area and functional groups of rGO. Xiao et al. [55] observed that in Ag_2O/TiO_2/rGO composites, superoxide anions ($\bullet O_2^-$) play a key role, with rGO acting as an electron transport channel to promote ROS generation and suppress carrier recombination, thus enhancing photocatalytic performance. However, comparing these results is challenging due to variations in experimental conditions, catalyst properties, illumination source and the potential photosensitization effects of RhB, which complicate the precise identification of catalytic mechanisms [56].

4. Conclusion

In conclusion, V_2O_5 nanorods decorated with RGO layers via a hydrothermal method were successfully synthesized and used for the photocatalytic degradation of Rhodamine-B dye. Characterization techniques such as XRD, SEM, and Raman confirmed the formation of V_2O_5/RGO nanocomposites. The functionalization with RGO reduced the band gap of V_2O_5, attributed to interfacial interactions between the two components. DFT study showed substantial interfacial binding and charge transfer, enhancing the electronic properties. Combined with improved charge separation and reactive oxygen species generation, these characteristics underline the hybrid's potential for effective Rhodamine-B photocatalytic and other applications in catalysis. The V_2O_5/RGO photocatalyst demonstrated a significant increase in RhB degradation efficiency (82 % in 240 min) compared to pure V_2O_5 (60 %). Integrating the two materials improved the charge-transport property and promoted the separation of photogenerated charge carriers.

CRediT authorship contribution statement

Issam Boukhoubza: Writing – review & editing, Writing – original draft, Visualization, Methodology, Investigation, Formal analysis, Data curation, Conceptualization. **Mohamed Achehboune:** Writing – review & editing, Writing – original draft, Software, Formal analysis. **Outman**

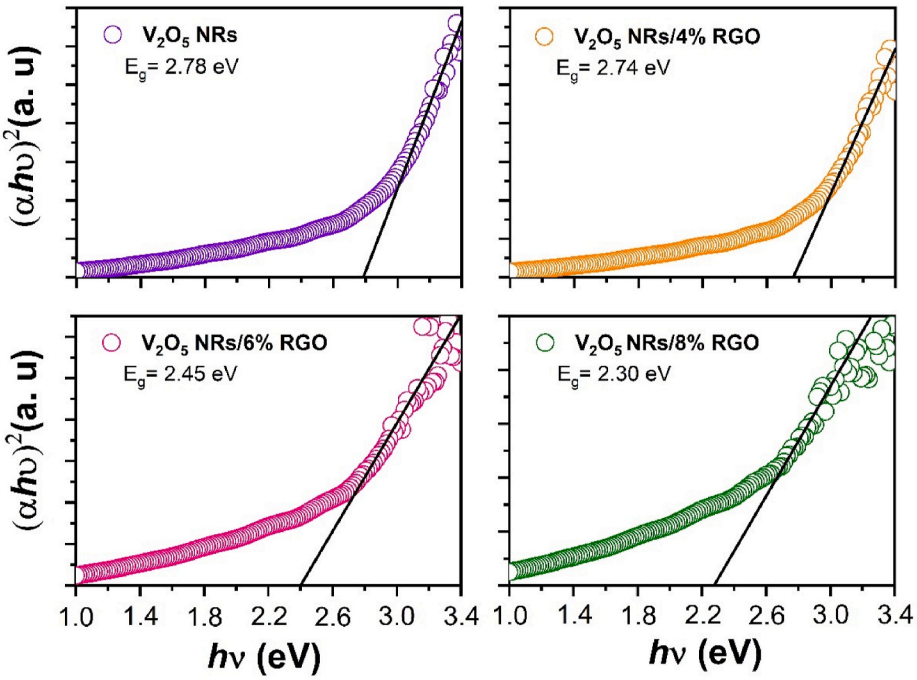

Fig. 8. Tauc plots for estimating the bandgap of V_2O_5 NRs and V_2O_5 NRs/RGO nanocomposites with different concentrations of RGO.

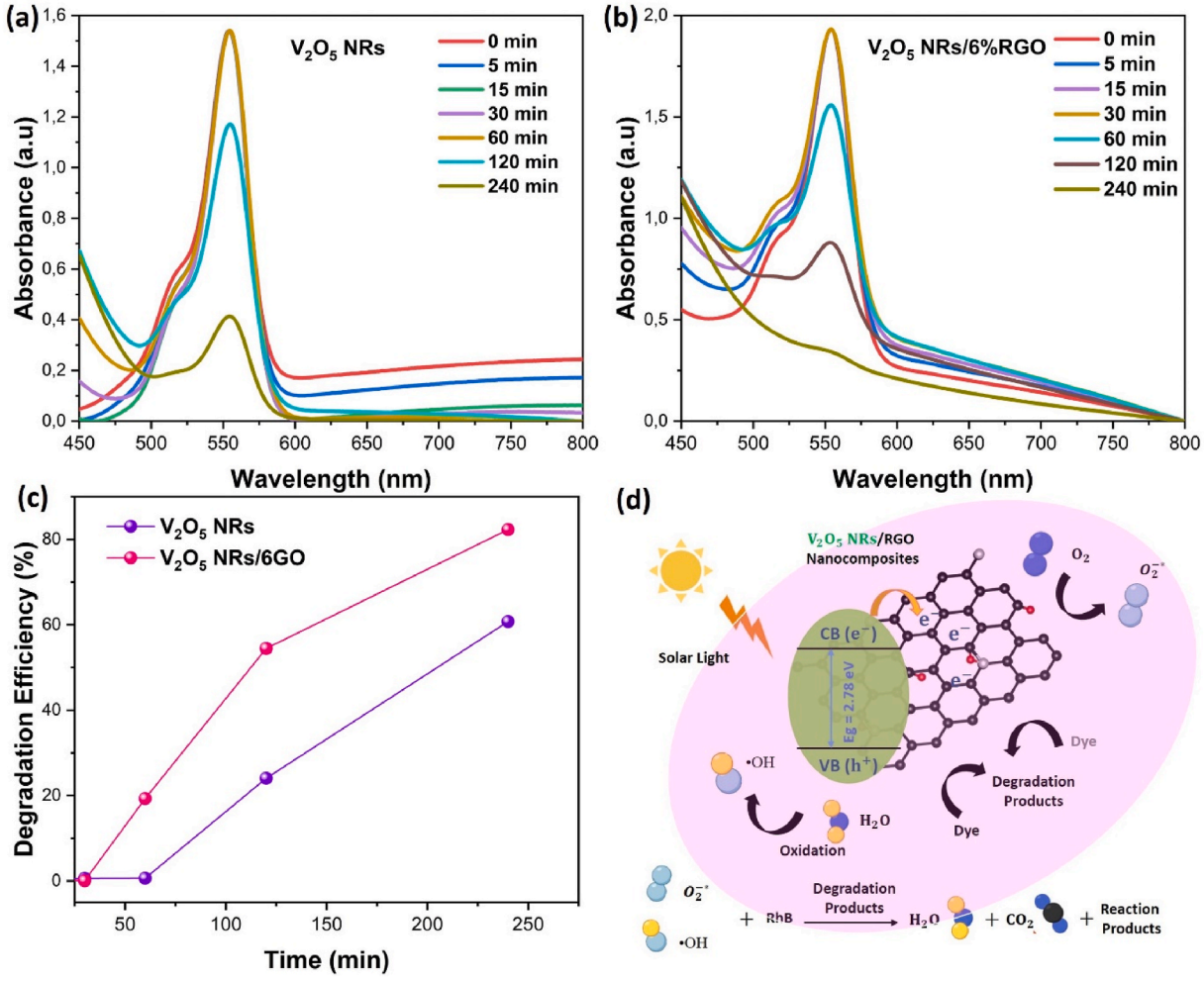

Fig. 9. Absorption spectra of RhB solutions after irradiation with visible light of a solar simulator for different times in the presence of (a) V_2O_5 NRs, (b) V_2O_5 NRs/6%RGO nanocomposites, (c) Degradation efficiency of V_2O_5 NRs and V_2O_5 NRs/6%RGO and (d) Schematic illustration of the mechanism of photocatalytic activity.

Table 3
Photocatalytic degradation of V_2O_5/RGO nanocomposites reported by previous studies.

Material	Synthesis Method	Dye	Light Source	Degradation Efficiency	Theoritical results	Ref.
Nb–V_2O_5: rGO	Hydrothermal	MB	Visible light	31 %, 75 min	–	[50]
rGO-V $_2O_5$	Sol gel and sonochemical	MB	UV–Visible light	71 %, 20 min	–	[51]
V_2O_5/RGO	Hydrothermal	MB	UV–Visible light	85 %, 255min	–	[52]
V_2O_5/RGO	Advanced Oxidation Process	Rh–B	Sunlight	84 %, 50 min	–	[5]
V_2O_5/RGO	Hydrothermal	Rh–B	Solar light	82 %, 240 min	High V_2O_5-RGO interaction and charge Transfer	This work

El Khouja: Investigation. **Mohamed A. Basyooni-M. Kabatas:** Software. **Melania Mindroc:** Investigation. **Issam Derkaoui:** Visualization, Investigation. **Monica Enculescu:** Visualization, Resources, Methodology, Investigation, Conceptualization. **Elena Matei:** Writing – review & editing, Visualization, Validation, Supervision, Resources, Project administration, Methodology, Investigation, Funding acquisition, Conceptualization.

Declaration of competing interest

The authors declare that they have no known competing financial interests or personal relationships that could have appeared to influence the work reported in this paper.

Acknowledgments

I.B. acknowledges the Romanian Ministry of Foreign Affairs and the Agence Universitaire de la Francophonie (AUF) for the Eugen Ionescu research and mobility grant at the National Institute of Materials Physics. M.A gratefully acknowledges the Consortium des Équipements de Calcul Intensif (CÉCI), funded by the Fonds de la Recherche Scientifique de Belgique (F.R.S.-FNRS) and the Wallon region (Conventions No. 2.5020.11, GEQ U.G006.15, 1610468, RW/GEQ2016 and U.G011.22) for providing Computational resources. E.M acknowledge financial support from EU under Romanian Recovery and Resilience Plan PNRR, Pillar III, Component C9–I8, contract nr.760083/May 23, 2023 and M.E acknowledge Core Program of the National Institute of Materials Physics, granted by the Romanian Ministry of Research, Innovation and Digitalization under the Project PC1-PN23080101.

Data availability

Data will be made available on request.

References

[1] E. Aawani, N. Memarian, H.R. Dizaji, Synthesis and characterization of reduced graphene oxide–V2O5 nanocomposite for enhanced photocatalytic activity under different types of irradiation, J. Phys. Chem. Solid. 125 (2019) 8–15.
[2] H. Tahir, M. Saad, Using dyes to evaluate the photocatalytic activity, in: Interface Sci. Technol., Elsevier, 2021, pp. 125–224.
[3] Y. Hirami, Y.M. Hunge, N. Suzuki, V. Rodríguez-González, T. Kondo, M. Yuasa, A. Fujishima, K. Teshima, C. Terashima, Enhanced degradation of ibuprofen using a combined treatment of plasma and Fenton reactions, J. Colloid Interface Sci. 642 (2023) 829–836, https://doi.org/10.1016/j.jcis.2023.02.136.
[4] A.A. Yadav, Y.M. Hunge, S.-W. Kang, A. Fujishima, C. Terashima, Enhanced photocatalytic degradation activity using the V2O5/RGO composite, Nanomaterials 13 (2023) 338.
[5] P.S. Chauhan, K. Kumar, K. Singh, S. Bhattacharya, Fast decolorization of rhodamine-B dye using novel V2O5-rGO photocatalyst under solar irradiation, Synth. Met. 283 (2022) 116981.
[6] V. Kale, Y.M. Hunge, S.A. Kamble, M. Deshmukh, S.V. Bhoraskar, V.L. Mathe, Modification of energy level diagram of nano-crystalline ZnO by its composites with ZnWO4 suitable for sunlight assisted photo catalytic activity, Mater. Today Commun. 26 (2021) 102101.
[7] A.A. Yadav, Y.M. Hunge, S.B. Kulkarni, Synthesis of multifunctional FeCo2O4 electrode using ultrasonic treatment for photocatalysis and energy storage applications, Ultrason. Sonochem. 58 (2019) 104663.
[8] A.A. Yadav, Y.M. Hunge, V.L. Mathe, S.B. Kulkarni, Photocatalytic degradation of salicylic acid using BaTiO3 photocatalyst under ultraviolet light illumination, J. Mater. Sci. Mater. Electron. 29 (2018) 15069–15073, https://doi.org/10.1007/s10854-018-9646-3.
[9] Y.M. Hunge, A.A. Yadav, S. Liu, V.L. Mathe, Sonochemical synthesis of CZTS photocatalyst for photocatalytic degradation of phthalic acid, Ultrason. Sonochem. 56 (2019) 284–289.
[10] Y.M. Hunge, A.A. Yadav, S.-W. Kang, Photocatalytic degradation of eriochrome black-T using BaWO4/MoS2 Composite, Catalysts 12 (2022) 1290.
[11] R. Jain, M. Mathur, S. Sikarwar, A. Mittal, Removal of the hazardous dye rhodamine B through photocatalytic and adsorption treatments, J. Environ. Manag. 85 (2007) 956–964.
[12] P. Bartasun, H. Cieśliński, A. Bujacz, A. Wierzbicka-Woś, J. Kur, A study on the interaction of rhodamine B with methylthioadenosine phosphorylase protein sourced from an Antarctic soil metagenomic library, PLoS One 8 (2013) e55697.
[13] D.B. McGregor, A.G. Brown, S. Howgate, D. McBride, C. Riach, W.J. Caspary, J. H. Carver, Responses of the L5178Y mouse lymphoma cell forward mutation assay. V: 27 coded chemicals, Environ. Mol. Mutagen. 17 (1991) 196–219, https://doi.org/10.1002/em.2850170309.
[14] J.C. Mirsalis, C.K. Tyson, K.L. Steinmetz, E.K. Loh, C.M. Hamilton, J.P. Bakke, J. W. Spalding, Measurement of unscheduled DNA synthesis and S-phase synthesis in rodent hepatocytes following in vivo treatment: testing of 24 compounds, Environ. Mol. Mutagen. 14 (1989) 155–164, https://doi.org/10.1002/em.2850140305.
[15] E. Grabowska, M. Marchelek, M. Paszkiewicz-Gawron, A. Zaleska-Medynska, Metal oxide photocatalysts. https://repozytorium.bg.ug.edu.pl/info/article/UOG2a4bb515cda247df884699bcf46cacc7/, 2018. (Accessed 4 October 2024).
[16] S. Bansal, A. Singh, D. Poddar, P. Jain, Fabrication and photocatalytic evaluation of functionalized chitosan decorated vanadium pentoxide nano-adsorbents for water remediation, Ceram. Int. 49 (2023) 8871–8885.
[17] L.A. Ivanov, L.D. Xu, Z.V. Pisarenko, S.R. Muminova, N.G. Miloradova, Inventions in the area of nanotechnologies and nanomaterials. Part I, Nanotechnol. Construction: A Sci. Internet-J. 15 (2023). https://digitalcommons.odu.edu/itds_facpubs/86/. (Accessed 15 January 2025).
[18] S. Le, C. Zhu, Y. Cao, P. Wang, Q. Liu, H. Zhou, C. Chen, S. Wang, X. Duan, V2O5 nanodot-decorated laminar C3N4 for sustainable photodegradation of amoxicillin under solar light, Appl. Catal. B Environ. 303 (2022) 120903.
[19] S.K. Jayaraj, V. Sadishkumar, T. Arun, P. Thangadurai, Enhanced photocatalytic activity of V2O5 nanorods for the photodegradation of organic dyes: a detailed understanding of the mechanism and their antibacterial activity, Mater. Sci. Semicond. Process. 85 (2018) 122–133.
[20] P.S. Chauhan, A. Mishra, G. Bhatt, S. Bhattacharya, Enhanced He gas detection by V2O5-noble metal (Au, Ag, and Pd) nanocomposite with temperature dependent n-to p-type transition, Mater. Sci. Semicond. Process. 123 (2021) 105528.
[21] X. Zou, J. Zhang, X. Zhao, Z. Zhang, MoS2/RGO composites for photocatalytic degradation of ranitidine and elimination of NDMA formation potential under visible light, Chem. Eng. J. 383 (2020) 123084.
[22] V.L. Siong, C.W. Lai, J.C. Juan, K.M. Lee, B.F. Leo, C.S. Khe, One-step solvothermal synthesis of rGO/TiO2 nanocomposite for efficient solar photocatalytic degradation of methylene blue dye, Curr. Nanosci. 15 (2019) 157–162.
[23] I. Boukhoubza, M. Khenfouch, M. Achehboune, B. Mothudi, I. Zorkani, A. Jorio, Synthesis and characterization of Graphene oxide/Zinc oxide nanorods sandwich structure, J. Phys. Conf. Ser. (2018) 012005. IOP Publishing, https://iopscience.iop.org/article/10.1088/1742-6596/984/1/012005/meta. (Accessed 4 October 2024).
[24] T.K. Le, M. Kang, S.W. Kim, Relation of photoluminescence and sunlight photocatalytic activities of pure V2O5 nanohollows and V2O5/RGO nanocomposites, Mater. Sci. Semicond. Process. 100 (2019) 159–166.
[25] D. Sharma, M. Faraz, D. Kumar, D. Takhar, B. Birajdar, N. Khare, Visible light activated V2O5/rGO nanocomposite for enhanced photodegradation of methylene blue dye and photoelectrochemical water splitting, Inorg. Chem. Commun. 142 (2022) 109657.
[26] D.-T. Tran, T.-H. Ha, V.-N. Nguyen, T.-D. Pham, Novel CeO2-V2O5/rGO tertiary photocatalyst for improved cefotaxime degradation using visible-light, Inorg. Chem. Commun. 161 (2024) 112044.
[27] M. Zou, W. Wen, J. Li, H. Lai, Z. Huang, Electric Cu nanoparticles decorated V2O5 spheres as high performance cathodes for lithium ion batteries, J. Alloys Compd. 681 (2016) 268–274.
[28] G. Kresse, J. Furthmüller, Efficient iterative schemes for ab initio total-energy calculations using a plane-wave basis set, Phys. Rev. B 54 (1996) 11169–11186.
[29] G. Kresse, D. Joubert, From ultrasoft pseudopotentials to the projector augmented-wave method, Phys. Rev. B 59 (1999) 1758–1775.
[30] P.E. Blöchl, Projector augmented-wave method, Phys. Rev. B 50 (1994) 17953–17979.
[31] M. Ernzerhof, G.E. Scuseria, Assessment of the perdew–burke–ernzerhof exchange-correlation functional, J. Chem. Phys. 110 (1999) 5029–5036.
[32] S. Grimme, Semiempirical GGA-type density functional constructed with a long-range dispersion correction, J. Comput. Chem. 27 (2006) 1787–1799.
[33] R.F.W. Bader, Atoms in molecules, Acc. Chem. Res. 18 (1985) 9–15.

[34] J. Pan, L. Zhong, M. Li, Y. Luo, G. Li, Microwave-Assisted solvothermal synthesis of VO $_2$ hollow spheres and their conversion into V $_2$ O $_5$ hollow spheres with improved lithium storage capability, Chem. Eur J. 22 (2016) 1461–1466.
[35] N.M. Abd-Alghafour, N.M. Ahmed, Z. Hassan, Fabrication and characterization of V2O5 nanorods based metal–semiconductor–metal photodetector, Sens. Actuators Phys. 250 (2016) 250–257.
[36] N. Rama, M.R. Rao, Synthesis and study of electrical and magnetic properties of vanadium oxide micro and nanosized rods grown using pulsed laser deposition technique, Solid State Commun. 150 (2010) 1041–1044.
[37] S. De, A. Dey, S.K. De, Electrical transport and optical properties of vanadyl phosphate—polyaniline nanocomposites, J. Phys. Chem. Solid. 68 (2007) 66–72.
[38] I. Derkaoui, M. Khenfouch, I. Boukhoubza, M. Achehboune, R. Hatel, B. M. Mothudi, I. Zorkani, A. Jorio, ·M. Maaza, Microwave assisted growth of highly oriented vanadium oxides nanostructures: structural, vibrational and electrical properties, Appl. Phys. A 127 (2021) 934.
[39] D. Nath, F. Singh, R. Das, X-ray diffraction analysis by Williamson-Hall, Halder-Wagner and size-strain plot methods of CdSe nanoparticles- a comparative study, Mater. Chem. Phys. 239 (2020) 122021.
[40] S. Rajeshwari, J.S. Kumar, R.T. Rajendrakumar, N. Ponpandian, P. Thangadurai, Influence of Sn ion doping on the photocatalytic performance of V2O5 nanorods prepared by hydrothermal method, Mater. Res. Express 5 (2018) 025507.
[41] X. Wang, C. Zuo, L. Jia, Q. Liu, X. Guo, X. Jing, J. Wang, Synthesis of sandwich-like vanadium pentoxide/carbon nanotubes composites for high performance supercapacitor electrodes, J. Alloys Compd. 708 (2017) 134–140.
[42] J. Chen, B. Yao, C. Li, G. Shi, An improved Hummers method for eco-friendly synthesis of graphene oxide, Carbon 64 (2013) 225–229.
[43] Z. Bo, X. Shuai, S. Mao, H. Yang, J. Qian, J. Chen, J. Yan, K. Cen, Green preparation of reduced graphene oxide for sensing and energy storage applications, Sci. Rep. 4 (2014) 1–8.
[44] F. Tuinstra, J.L. Koenig, Raman spectrum of graphite, J. Chem. Phys. 53 (1970) 1126–1130.
[45] I. Boukhoubza, E. Matei, A. Jorio, M. Enculescu, I. Enculescu, Electrochemical deposition of ZnO nanowires on CVD-graphene/copper substrates, Nanomaterials 12 (2022) 2858.
[46] G. Silversmit, D. Depla, H. Poelman, G.B. Marin, R. De Gryse, Determination of the V2p XPS binding energies for different vanadium oxidation states (V5+ to V0+), J. Electron. Spectrosc. Relat. Phenom. 135 (2004) 167–175.
[47] X. Zhang, X. Liu, C. Yang, N. Li, T. Ji, K. Yan, B. Zhu, J. Yin, J. Zhao, Y. Li, A V2O5-nanosheets-coated hard carbon fiber fabric as high-performance anode for sodium ion battery, Surf. Coating. Technol. 358 (2019) 661–666.
[48] X. Wang, Y. Huang, D. Jia, W.K. Pang, Z. Guo, Y. Du, X. Tang, Y. Cao, Self-assembled sandwich-like vanadium oxide/graphene mesoporous composite as high-capacity anode material for lithium ion batteries, Inorg. Chem. 54 (2015) 11799–11806.
[49] S. Shafique, S. Yang, T. Iqbal, B. Cheng, Y. Wang, H. Sarwar, Y.T. Woldu, P. Ji, Improving the performance of V2O5/rGO hybrid nanocomposites for photodetector applications, Sens. Actuators Phys. 332 (2021) 113073.
[50] L. Bravo-Avellaneda, L. Moreno-Aldana, L.J. Cardenas-Flechas, Enhancing photocatalytic degradation with V_2O_5-based catalysts: integrating niobium and graphene oxide, Emergent Mater (2025), https://doi.org/10.1007/s42247-024-00932-6.
[51] A. Mishra, A. Panigrahi, P. Mal, S. Penta, G. Padmaja, G. Bera, P. Das, P. Rambabu, G.R. Turpu, Rapid photodegradation of methylene blue dye by rGO-V_2O_5 nano composite, J. Alloys Compd. 842 (2020) 155746.
[52] E. Aawani, N. Memarian, H.R. Dizaji, Synthesis and characterization of reduced graphene oxide–V2O5 nanocomposite for enhanced photocatalytic activity under different types of irradiation, J. Phys. Chem. Solid. 125 (2019) 8–15.
[53] D. Sharma, M. Faraz, D. Kumar, D. Takhar, B. Birajdar, N. Khare, Visible light activated V2O5/rGO nanocomposite for enhanced photodegradation of methylene blue dye and photoelectrochemical water splitting, Inorg. Chem. Commun. 142 (2022) 109657.
[54] L.Z. Pei, N. Lin, T. Wei, H.D. Liu, H.Y. Yu, Zinc vanadate nanorods and their visible light photocatalytic activity, J. Alloys Compd. 631 (2015) 90–98.
[55] H. Xiao, T. Wang, Graphene oxide (rGO)-metal oxide (TiO_2/Ag_2O) based nanocomposites for the removal of rhodamine B at UV–visible light, J. Phys. Chem. Solid. 154 (2021) 110100.
[56] N. Memarian, E. Farahi, N. Tobeiha, S. You, I. Concina, Understanding graphitic carbon nitride as photocatalyst: a case study on thermal engineering of physical and chemical features, Phys. Status Solidi 221 (2024) 2300844.